2020

Ultrathin Few-Layer GeP Nanosheets via Lithiation-Assisted Chemical Exfoliation and Their Application in Sodium Storage

Fuhua Yang
University of Wollongong, fy896@uowmail.edu.au

Jian Hong
University of Wollongong

Junnan Hao
University of Wollongong, jh845@uowmail.edu.au

Shilin Zhang
University of Wollongong, sz384@uowmail.edu.au

Gemeng Liang
University of Wollongong, gl906@uowmail.edu.au

See next page for additional authors

Ultrathin Few-Layer GeP Nanosheets via Lithiation-Assisted Chemical Exfoliation and Their Application in Sodium Storage

Abstract

2020 WILEY-VCH Verlag GmbH & Co. KGaA, Weinheim Ultrathin few-layer materials have attracted intensive research attention because of their distinctive and unique properties. Few-layer GeP (FL-GP) is potentially interesting for application in electronics and optoelectronics because of its appropriate band gap and good stability under ambient conditions. Nevertheless, it is a challenge to achieve ultrathin few-layer or single layer GeP from exfoliation of bulk crystals. Here, a lithiation-assisted chemical exfoliation technique is employed to achieve FL-GP, in which the interlayer spacing can be efficiently enlarged after a preliminary lithium ion intercalation, allowing the bulk crystal to be readily exfoliated in a following ultrasonication. As a result, ultrathin FL-GP is obtained. In a demonstration, the FL-GP/reduced graphene oxide (rGO) demonstrates remarkable sodium storage performance. The FL-GP with a two-dimensional structure shortens the ion transport pathways and alleviates the volume variation during sodiation. Meanwhile, the rGO in the composite improves the conductivity of the whole electrode. The as-prepared FL-GP/rGO electrode exhibits a high capacity of 504.2 mAh g−1 at 100 mA g−1, remarkable rate performance, and superior cycling stability in the half cells. FL-GP/rGO//Na3V2(PO4)3 full cells are also assembled and demonstrated satisfactory electrochemical performance, indicating potential application of the as-prepared anode materials.

Disciplines

Engineering | Science and Technology Studies

Publication Details

Yang, F., Hong, J., Hao, J., Zhang, S., Liang, G., Long, J., Liu, Y., Liu, N., Pang, W., Chen, J. & Guo, Z. (2020). Ultrathin Few-Layer GeP Nanosheets via Lithiation-Assisted Chemical Exfoliation and Their Application in Sodium Storage. Advanced Energy Materials,

Authors

Fuhua Yang, Jian Hong, Junnan Hao, Shilin Zhang, Gemeng Liang, Jun Long, Yuqing Liu, Nana Liu, Wei Kong Pang, Jun Chen, and Zaiping Guo

Ultrathin few-layer GeP nanosheets via lithiation-assisted chemical exfoliation and their application in sodium storage

*Fuhua Yang [a], Jian Hong [a], Junnan Hao [a], Shilin Zhang [a], Gemeng Liang[a], Jun Long [a], Yuqing Liu [b], Nana Liu [a], Wei Kong Pang [a], Jun Chen [b *], Zaiping Guo [a *]*

[a] Institute for Superconducting and Electronic Materials, School of Mechanical, Materials, Mechatronics and Biomedical Engineering, University of Wollongong, North Wollongong, NSW 2522, Australia. E-mail: zguo@uow.edu.au

[b] ARC Centre of Excellence for Electromaterials Science, Intelligent Polymer Research Institute, Australian Institute of Innovative Materials, University of Wollongong, North Wollongong, NSW 2522, Australia. E-mail: junc@uow.edu.au

Keywords: 2D materials, germanium phosphide, sodium storage, chemical exfoliation

Abstract

Ultrathin few-layer materials have attracted intensive research attention because of their distinctive and unique properties. Few-layer GeP (FL-GP) is potentially interesting for application in electronics and optoelectronics because of its appropriate band gap and good stability under ambient conditions. Nevertheless, it is a challenge to achieve ultrathin few-layer or single layer GeP from exfoliation of bulk crystals. Here, a lithiation-assisted chemical exfoliation technique is employed to achieve FL-GP, in which the interlayer spacing can be efficiently enlarged after a preliminary lithium ion intercalation, allowing the bulk crystal to be readily exfoliated in a following ultrasonication. As a result, ultrathin FL-GP is obtained. In a demonstration, the FL-GP/reduced graphene oxide (rGO) has manifested remarkable sodium storage performance. The FL-GP with two-dimensional structure shortens the ion transport pathways and alleviates the volume variation during the sodiation. Meanwhile, the rGO

in the composite improves the conductivity of the whole electrode. The as-prepared FL-GP/rGO electrode exhibits a high capacity of 504.2 mAh g^{-1} at 100 mA g^{-1}, remarkable rate performance (with a reversible capacity of 230 mAh g^{-1} retained at 2 A g^{-1}), and superior cycling stability (with a reversible capacity of 230 mAh g^{-1} still retained after 250 cycles at 1 A g^{-1}) in the half cells. FL-GP/rGO//$Na_3V_2(PO_4)_3$ full cells have also been assembled and demonstrated satisfactory electrochemical performance, indicating potential application of the as-prepared anode materials.

1. Introduction

Two-dimensional (2D) materials with an appropriate band gap have attracted tremendous attention during the past few decades due to their unique physical and chemical properties compared to their bulk counterparts[1][2][3][4][5]. For applications involving the emission/absorption of photons, such as lasers, light emitting diodes (LEDs), and solar cells, it is essential for the materials to possess an appropriate band gap. Graphene, the first discovered and most studied 2D material, however, lacks an intrinsic band gap, and thus, its further application is limited[6][7][8]. Phosphorene, another attractive 2D material, despite possessing a band gap of ~1.5 eV, is unstable and sensitive to water and oxygen, stifling any widespread use [9][10][11]. Therefore, it is of great importance to develop new 2D materials with appropriate band gaps and stability under ambient conditions. Few-layer GeP (FL-GP) should be a good 2D material candidate, not only because of its layer-dependent indirect band gap, varying from 1.68 eV for a monolayer to 0.51 eV for the bulk, but also its good stability under

ambient conditions[12][13]. As a result, FL-GP should have the potential to perform in a wide range of applications for electronics and optoelectronics[14]. In particular, GeP has already been fabricated into electrodes for rechargeable lithium/sodium batteries, not only because of its relatively high conductivity, but also its high theoretical capacity, as well as its appropriate low redox potential, although the large size of the bulk particles resulted in fast capacity fading[15]. Previous reports have proofed than nanostructured materials are favorable to enhance the electrochemical performance.[16][17][18] Trimming the particle size of the bulk GeP down to 2D nanosheets could offer a large contact area between the active materials and the electrolyte, short electron and ion transport paths, and also sufficient active sites for lithium/sodium storage, which are favorable for high electrochemical performance[19][20]. Nevertheless, it is a challenge to achieve ultrathin few-layer or single-layer GeP from the exfoliation of bulk crystals.

Similar to black phosphorus, bulk GeP consists of puckered sheets held together by weak van der Waals forces, allowing it to be readily cleaved along the layer surface to yield 2D nanosheets[12][21][14]. Li et al. first introduced GeP nanosheets into the growing 2D materials family by exfoliating bulk GeP using a mechanical exfoliation method[12]. The reported GeP nanosheets, however, possess a thickness ranging from 4.3-11.7 nm. The high thickness of the 2D material would definitely compromise the advantages of the 2D nanostructure. To synthesize ultrathin FL-GP, more effort was needed. The synthesis techniques for ultrathin 2D materials include chemical vapor deposition (CVD)[22], shear exfoliation[23], and direct exfoliation[24]. Previous reports have revealed, however, that lithiation-assisted chemical exfoliation is an efficient method[25][26]. The

interlayer spacing can be efficiently enlarged by the preliminary lithium ion intercalation, allowing the bulk crystal to be readily exfoliated in the following ultrasonication.

In this work, FL-GP was synthesized using a lithiation-assisted chemical exfoliation technique, in which *N*-butyllithium was used as lithium donor. The as-prepared FL-GP had an average thickness of 4.54 nm. As an example, we demonstrate the use of the FL-GP as anode material for sodium ion batteries by combining them with highly conductive reduced graphene oxide (rGO). The ultrathin nanosheets dramatically shorten the electron/sodium ion transport paths and efficiently address the fatal issue of volume changes for GeP during the charge-discharge process, which would result in fast capacity decay. Furthermore, the relatively poor electrical conductivity of pure GeP is enhanced by incorporating a small amount of rGO. As a result, the electrochemical properties were greatly improved, with a high reversible capacity of 504.2 mAh g^{-1} retained after 70 cycles at 100 mA g^{-1}. Even at the high current density of 2 A g^{-1} in the rate performance test, a capacity of 250 mAh g^{-1} was achieved. What is more, the $Na_3V_2(PO_4)$//FL-GP/rGO full cell demonstrated a specific capacity of 185 mAh g^{-1} after 100 cycles at 1 A g^{-1}, pointing to the potential application of ultrathin FL-GP/rGO in high-energy-density sodium ion batteries. To the best of our knowledge, this is the first report on the synthesis of ultrathin FL-GP and its electrochemical performance. We believe that our work will provide new insights to attract and promote more attention to this promising anode material.

2. Experimental section

2.1.Materials synthesis

Synthesis of bulk GeP crystals[12][21]: The starting materials, Ge, P, and Bi, were first weighed out in the molar ratio of 1:2:5, respectively. The mixture was loaded into a small quartz tube, which was then evacuated and sealed. The quartz tube was heated up to a high temperature of 950 ^{o}C with a heating rate of 5 ^{o}C min^{-1} and held at that temperature for 24 h before it was slowly cooled down to 600 ^{o}C at 2 ^{o}C h^{-1}. In order to force the excess Bi metal flux off of the GeP crystals, the quartz tube was taken out of the furnace at 600 ^{o}C and subjected to centrifugation while the product inside the quartz tube was still in the liquid state. After that, when the product cooled down to room temperature, the GeP crystals were separated from the Bi metal by mechanical exfoliation. The remaining traces of Bi were further removed by washing the sample in an HCl/H_2O_2 solution.

Synthesis of few-layer GeP (FL-GP): 1.5 g bulk GeP crystals were added into 10 mL of 1.5 M *n*-butyllithium in hexane solution. The solution was stirred in an argon-filled glove box for 96 h, and the suspension was then sealed in a centrifuge tube and taken out of glove box for centrifugation. After that, the clear liquor was discarded, while the Li-intercalated residue was collected and moved into the glove box for further treatment. The leftover *n*-butyllithium was further removed by washing the sample in hexane several times. The as-obtained sample was then dispersed into water again and sonicated using a tip probe ultrasonicator for 2 h, followed by centrifugation at 1000 rpm for 8 minutes. Then, the residue at the bottom was discarded, and the supernatant was collected and dried in a 60 ^{o}C oven to obtain the FL-GP.

Synthesis of FL-GP/rGO nanosheets: FL-GP and graphene oxide (GO) in a weight ratio of 10:1 were dispersed into deionized (DI) water in a sonic bath, and the suspension was then added dropwise into liquid nitrogen to freeze the sample. After freeze-drying and calcination of the sample at 500 ºC under argon atmosphere, the final FL-GP/rGO nanosheets were obtained.

The $Na_3V_2(PO_4)_3$ were synthesized by a one-step solid state reaction as follows: the stoichiometric $NaH_2PO_4{\cdot}2H_2O$ and V_2O_3 powders were put in the agate jar as precursors and then the precursors were ball-milled in a planetary ball mill at 400 rpm in a stainless steel vessel for 8 h. After ball milling, the mixture was pressed into a pellet and then heated at 900 °C for 24 h in Ar atmosphere.

2.2. Materials characterization:

The crystal structures of the as-prepared samples were studied by X-ray diffraction (XRD, GBC MMA diffractometer) with Cu Kα radiation (λ = 1.54056 Å) at a scanning rate of 1º min^{-1}. Field-emission scanning electron microscopy (FESEM, JEOL JSM-7500FA) and scanning transmission electron microscopy (STEM, JEOL JEM-ARM200F) were employed to investigate the morphology of the products. Investigation of the details of the crystal structure and energy dispersive spectroscopy (EDS) mapping were further conducted by STEM at 200 kV. X-ray photoelectron spectroscopy (XPS) experiments were carried out using a VG multilab 2000 (VG Inc.), and all the binding energy data were calibrated using the C 1s peak at 284.8 eV of the surface adventitious carbon. The photoelectron spectrometer used monochromatic Al Kα radiation under vacuum of 2×10^{-6} Pa. Thermogravimetric analysis measurements (TGA; TA

Instruments 2000) were carried out under flowing air at a heating rate of 5 °C min^{-1} from room temperature to 700 °C. Raman spectra were collected on a JOBIN Yvon Horiba Raman spectrometer model HR800, using a 10 mW helium/neon laser at 632.8 nm excitation.

2.3. Electrochemical measurements

The working electrodes were prepared by a slurry-coating method. A mixture of the as-prepared sample, a conductive agent (Super P) and carboxymethyl cellulose (CMC) in a weight ratio of 8:1:1 was first ground in DI water to produce a slurry. Then, the slurry was spread onto copper foil with a doctor blade before the foil was dried in an 80 °C evacuated oven overnight. After that, the copper foil loaded with the electrode materials was cut into small disks for battery assembly later on. The loading mass of the active materials was estimated to be around 1.0 mg cm^{-2}. Battery assembly was carried out in a glove box with oxygen and moisture levels below 0.1 ppm. For the SIBs half cells, a sodium disk and glass fiber (Whatman) were respectively used as the counter electrode and separator, and the electrolyte was 1 M $NaClO_4$ in ethylene carbonate (EC)/diethyl carbonate (DEC) (1:1 by volume) with 5% fluoroethylene carbonate (FEC). For the lithium ion batteries assemble, the counter electrode was a disk of lithium metal, and Celgard 2400 were used as separator. The electrolyte was 1 M $LiPF_6$ in ethylene carbonate (EC)/diethyl carbonate (DEC) (1:1 by volume). Cyclic voltammetry was carried out on a VMP-3 electrochemical workstation at different scan rates. The charge-discharge tests were conducted on a Land CT2001A battery tester over the voltage range of 0.01-2.5 V at different constant current densities. For the full cell $Na_3V_2(PO_4)$//FL-

GP/rGO batteries, the voltage range was from 1.0 to 3.75 V. In addition, to ensure material utilization and reasonably evaluate the electrochemical performance of FL-GP/rGO, full cells were assembled based on a capacity ratio of about 1:1.2 between the FL-GP/rGO anode and the $Na_3V_2(PO_4)$ cathode, and the cell capacity was calculated based on the weight of the anode material only in this work. The FL-GP/rGO was initially sodiated to 0.01 V with lithium foil as counter electrode, and then it was desodiated to 2.5 V. The activation procedure needed to be repeated three times under the current density of 50 mA g^{-1}. The discharge capacity of all the batteries is calculated based on the total mass of FL-GP/rGO.

3. Results and discussion

The overall synthesis procedure for the FL-GP/rGO is shown in Figure 1a. The as-prepared bulk GeP crystals with a layered structure (Figure S1 in the Supporting Information) were first treated in *n*-butyllithium/hexane solution, during which, the lithium ions coming from the *n*-butyllithium were intercalated between the GeP layers and enlarged the layer spacing[27]. Then, the lithium intercalated GeP was collected and dispersed in DI water again for a subsequent sonication treatment. The lithium-intercalated GeP crystal was mechanically exfoliated into 2D nanosheets during the sonication. In the last step, to further improve the conductivity of the composite, the FL-GP was combined with GO, and then the mixture was subjected to high temperature heating in argon in order to reduce the GO to rGO and yield the final product, FL-GP/rGO. The successful exfoliation of the GeP crystals was achieved by the lithium intercalation process. The chemical reaction between GeP and $Li^+(n\text{-}Bu)^-$ leads to the

electron transfer from Bu^- to GeP sheets. The Li^+ ions then intercalate to balance the charge which expand the lattice to a larger extent and form LixGeP. Exfoliation of LixGeP into individual GeP nanosheets is achieved by water addition (hydrolysis) and subsequent LiOH and hydrogen gas production between layers. Ultrasonication is employed at the hydrolysis step to improve the diffusion of hydroxyl groups and to facilitate the exfoliation[27][26]. To provide evidence of the FL-GP, a series of characterizations was carried out. As shown in Figure 1b, the Tyndall effect was demonstrated in the FL-GP sample when red light beams were incident from the sides of both the FL-GP suspension and the blank DI water, indicating good dispersibility of the FL-GP in the DI water[4]. Transmission electron microscope (TEM) images (Figure 1c) indicated that the ultrathin FL-GP nanosheets had a lateral size of several micrometers. Furthermore, atomic force microscopy (AFM) measurements were conducted to determine the exact thickness of the FL-GP. The results show (Figure 1d) that the thickness is around 1.6 nm, equivalent to two GeP layers[12]. The as-synthesis few-layer GeP thickness distribution histogram is shown in Figure S2. The typical thickness of the few-layer GeP nanosheets is mainly in the range of 1-7 nm and average thickness for the few-layer GeP nanosheets is calculated to be 4.54 nm.To the best of our knowledge, this is the first report on the successful synthesis of FL-GP. The FL-GP/rGO nanosheets were also imaged by TEM (Figure 1e), and a transparent and smooth 2D structure can be observed. The high-resolution TEM (HRTEM) image (Figure 1f) also demonstrates a *d*-spacing of 0.32 nm, which is ascribed to the (401) crystal planes. As a corresponding inset to the magnified TEM image, the fast Fourier

transform (FFT) pattern is consistent with the XRD pattern (as shown in Fig. 2). The characteristics of the graphene coating were also examined, and as is shown in the HRTEM image, the graphene tightly adhered to the surface of the FL-GP. The presence of the graphene would enhance the conductivity of the composite and improve the utilization coefficient of the active materials, thus achieving high reversible capacity. The element mapping verified that the Ge and P elements were evenly distributed and well correlated with the shape of the selected sample area. Apart from the Ge and P elements, C was also detected due to the coexistence of graphene.

Powder X-ray diffraction was used to identify the crystal structure of the bulk GeP and the FL-GP/rGO nanosheets. Figure 2a and b shows the satisfactory Rietveld refinement of bulk GeP and FL-GP/rGO with a good weighted profile R-factor of R_{wp} = 5.14% and R_{wp} = 4.30%, respectively. The diffraction peaks for the FL-GP/rGO can be indexed to monoclinic GeP with lattice parameters a = 15.12(3) Å, b = 3.658(3) Å, c = 9.17(1) Å, β = 101.57(6)°, and V = 497.3(5) Å^3. All the lattice parameters of FL-GP/rGO are similar to those of bulk GeP (a = 15.201(6) Å, b = 3.6285(8) Å, c = 9.184(2) Å, β = 101.52(1)°, and V = 496.3(3) Å^3). Trace amounts of Ge impurities (1.5%) were observed in the bulk GeP, and they turned to GeO_2 impurities in FL-GP/rGO. Raman measurements on the rGO, FL-GP, and FL-GP/rGO nanosheets were further carried out (Figure 2c). It can be seen from the resultant patterns that three peaks located at 200.8, 245.0, and 361.1 eV appear in both the FL-GP and the FL-GP/rGO samples. These three peaks are all from the GeP phase[13]. In addition, the Raman spectra of the rGO and FL-GP/rGO nanosheets both presented broad intense D and G bands of carbon. The

intensity ratio of the D to the G-band of FL-GP/rGO was calculated to be 1.3. Furthermore, the FL-GP/rGO nanosheets were also subjected to X-ray photoelectron spectroscopy (XPS) to examine their chemical compositions and surface electronic states. Figure 2d presents the high-resolution Ge 3d XPS spectrum, in which only one peak located at 31.3 eV is observed, which can be indexed to Ge 3d[12]. In Figure 2e, the two peaks at 131.2 and 130.6 eV can be assigned to P $2p_{1/2}$ and P $2p_{3/2}$, respectively, while the peak located at 127.8 eV is ascribed to the signal of Ge 3p[12]. The C 1s XPS spectrum of the FL-GP/rGO is shown in Figure 2f. The spectrum can be divided into three peaks: the strong peak at 284.7 eV is the signal of the non-oxygenated carbon (C-C/C=C), while the other two peaks located at 287.7 and 289.4 eV are indexed to C-O and O-C=O, respectively[28]. It is notable that the C-C/C=C peak signal is much more intense than those of C-O and O-C=O, which can be explained by the reduction of GO to rGO during the annealing process in argon. In order to determine the rGO content in the FL-GP/rGO nanosheet composite, thermogravimetric analysis (TGA) was carried out in air (Figure S3). The TGA curves show no weight change in the first 350 °C, but a weight increase is observed within the temperature window of 350-600 °C for the FL-GP/rGO nanosheets and 350-680 °C for the FL-GP, which can be ascribed to the oxidation of GeP to GeO_2 and P_2O_5. From calculations on the results for both samples, the rGO content of the FL-GP/rGO nanosheets is estimated to be 3.9%. Considering the relatively low capacity of rGO for sodium ion storage, a high content of rGO in the composite would compromise the capacity. On the other hand, a proper amount of rGO is necessary to improve the electrical conductivity and buffer the volume changes of

the FL-GP during cycling, thus enhancing the electrochemical performance.

Previous studies on GeP_3[29] and GeP_5[30] have confirmed that both Ge and P are sodium-reactive. Each P atom can electrochemically bond with three sodium atoms to form Na_3P, while a Ge atom can only react with one sodium ion to generate NaGe. According to this mechanism, the electrode reaction of GeP can be described by the following equation: $4Na^+ + 4e^- + GeP \leftrightarrow Na_3P + NaGe$. The theoretical capacity of GeP can be calculated to be 1035 mAh g^{-1}, in which the P contributes 776 mAh g^{-1} and the Ge contributes the other 259 mAh g^{-1} of capacity. Cyclic voltammetry (CV) measurements were conducted to reveal the above Na storage mechanism. As shown in Figure 3a, during the first negative scan, peaks arise between 0.25-0.7 V, which can be ascribed to the sodium reduction of the GeP and the formation of a solid electrolyte interphase (SEI) film. In the subsequent negative scans, three reduction peaks located at 0.63, 0.45, and 0.35 V are displayed, indicating a multi-step redox reaction process. The peak at 0.63 V can be assigned to the the intercalation reaction (GeP → Na_xGeP), while the peaks at 0.45 and 0.35 V are assigned to the further conversion (Na_xGeP → Ge + Na_3P) and alloying reactions (Ge → NaGe), respectively. Accordingly, the three oxidation peaks at 0.49, 0.66, and 0.79 V in the positive scan curves can be ascribed to the de-alloying, de-conversion, and de-intercalation reactions, respectively [15].

Charge-discharge measurements were carried out to investigate the sodium storage performance of the as-prepared samples. Figure 3d displays the charge-discharge curves of the FL-GP/rGO nanosheets at different current densities. At a current density of 100 mAh g^{-1}, the FL-GP/rGO nanosheets presented a high initial discharge capacity of 884.6

mAh g^{-1} and a charge capacity of 504.2 mAh g^{-1}, giving an initial Coulombic efficiency of 57%. The 43% irreversible capacity loss in the first cycle is mainly caused by the decomposition of electrolyte to form the surface SEI layer and the irreversible trapping of Na ions in the GeP lattice[31]. It is notable that, at all current densities, the working voltage of FL-GP/rGO is entirely below 1 V, which is favorable for achieving high energy density for the full cell. Figure 3e presents the cycling performances of both FL-GP/rGO and FL-GP nanosheets. As expected, thanks to the enhanced electronic conductivity, the FL-GP/rGO nanosheets managed to maintain a high reversible capacity of 504.2 mAh g^{-1} at the current density of 100 mA g^{-1} after 70 cycles without obvious capacity fading. In contrast, the pure FL-GP only demonstrated a reversible capacity of ~200 mAh g^{-1}, confirming the improved utilization of the active materials by the introduction of highly conductive graphene into the composite. Due to the unique properties of the 2D materials, both FL-GP/rGO and FL-GP exhibited better cycling stability than the bulk GeP, which suffered from fast capacity decay, with only ~50 mAh g^{-1} capacity remaining after 70 cycles (Figure S4). The fast capacity fading of the bulk GeP results from the large volume variation during the sodiation/desodiation process. A long-term cycling experiment on the FL-GP/rGO nanosheets conducted at a current density of 1 A g^{-1} showed that a reversible capacity of 230 mAh g^{-1} still remained after 250 cycles (Figure 3e). Rate performance testing was also carried out, as shown in Figure 3b and Figure S5, where the FL-GP/rGO presented higher rate capability than the FL-GP and bulk GeP at different current densities. A capacity of 570 mAh g^{-1} was achieved at 0.1 A g^{-1}, while 230 mAh g^{-1} was delivered at 2 A g^{-1}. To the best of our

knowledge, the rate performance of the FL-GP/rGO nanosheets is superior to those of most reported metal phosphides (Figure 3b inset)[32][33][34][35][36][37][38]. It is proposed that the remarkable cycling and rate performances of the FL-GP/rGO can be ascribed not only to the 2D structure (Figure S6), but also to the presence of the graphene with its ability to enhance the electron transfer rate. To confirm this point, electrochemical impedance spectroscopy (EIS) analysis was carried out to compare the FL-GP/rGO and FL-GP electrodes (Figure 3c). As expected, the interfacial resistance of the FL-GP/rGO nanosheets is smaller than that of the FL-GP, due to the presence of graphene to enhance the electronic conductivity. In addition, the FL-GP/rGO also showed satisfactory performance in lithium ion batteries, with a reversible capacity of 823 mAh g^{-1} sustained under 200 mA g^{-1} (Figure S7a and b).

Galvanostatic intermittent titration technique (GITT) measurements were conducted on a half cell in the third cycle to reach the thermal equilibrium state. The voltage responses of the FL-GP/rGO are presented in Figure 4a, and the ionic diffusion coefficients determined by the Fick's second law are displayed in the inset. The detailed calculation method is provided in the Supporting Information (Figure S8). As indicated in the results, the diffusion coefficients of the FL-GP/rGO nanosheets range from $10^{-11.1}$ to $10^{-9.4}$ cm^2 s^{-1} in the voltage range from 0.3 to 1.2 V, which is comparable to other reported anode materials[39][40]. The higher diffusion coefficients of the FL-GP/rGO nanosheets are favorable for improving the high-rate performance. In order to calculate the capacitance contribution, CV curves at different scan rates from 0.1 to 1.0 mV s^{-1} were collected and are presented in Figure 4b. All the curves show similar shapes, with both

redox peaks and a rectangular shape, suggesting that the Na^+ intercalation/deintercalation reaction and double-layer capacitive behavior are both included in the sodium storage mechanism[41]. It is well known that, for the alloying mechanism in anode materials, the faradaic process contributes the majority of the sodium ion storage, while the non-faradaic process contributes only a minority. To determine the contributions of both kinds of energy storage in the sodium storage mechanism, the *b* value was calculated from log-log curves of the peak current vs. the scan rate, as shown in Figure 4c. $b = 0.5$ indicates a faradaic process, and $b = 1$ suggests non-faradaic capacitive behavior. The results showed that the *b* values for the observed peaks are within the range of 0.76-0.86 (see the Supporting Information for the detailed calculation method), suggesting that both kinds of energy storage exist in the FL-GP/rGO nanosheets. Furthermore, Figure 4d presents the capacitance ratios of the total charge, in which the capacitance contribution is 40.7% at 0.1 mV s^{-1}. It is notable that the capacitance ratio increases gradually with the scan rate, and it reaches a value of 65.3% at 1 mV s^{-1}. The faradaic process is especially important for the anode material when it is working at a fixed low potential, and the non-faradaic process is favorable for enhanced rate capability with long cycling stability.

Thanks to its high reversible capacity, relatively low working voltage, and satisfactory cycling stability, the aforementioned FL-GP/rGO nanosheets should be a promising anode material for practical use. To confirm this point, prototype sodium-ion full cell batteries using FL-GP/rGO and $Na_3V_2(PO_4)_3$ as anode and cathode, respectively, were assembled, and their electrochemical performance was investigated (Figure 5a). The

$Na_3V_2(PO_4)_3$ cathode used in this work demonstrated similar phase structure to previous works (Figure S9) and demonstrated stable cycling performance, and a high reversible capacity of ~113 mAh g^{-1} was achieved in the half cells (Figure S10). As shown in Figure 5b, the $Na_3V_2(PO_4)_3$ cathode presents a very flat plateau at the voltage of ~3.7 V, while the working voltage window of the FL-GP/rGO anode was below 1 V. As expected, the $Na_3V_2(PO_4)_3$//FL-GP/rGO full cell demonstrated an average output voltage of about 2.5 V (Figure 5c), which is high enough to light up the LED bulb in Figure 5e. Figure 5d shows the cycling performance of the $Na_3V_2(PO_4)_3$//FL-GP/rGO full cell at a current density of 1 A g^{-1}. The as-assembled full cells delivered a high capacity of 307 mAh g^{-1} in the initial discharge, and a reversible capacity of 185 mAh g^{-1} was maintained after 100 cycles, giving a capacity retention of 60.3%. The performance of the FL-GP/rGO anode in the full cell is comparable with the other metal phosphide anodes (Table 1 in the supporting information).

This excellent electrochemical performance is due to the advantages of the FL-GP/rGO nanosheets. First, the ultrathin GeP nanosheets can shorten the electron/sodium ion transport paths, which is favorable for high rate performance. Second, the 2D materials could not only offer a large contact area between the active materials and the electrolyte, and provide sufficient active sites for sodium storage, but also could alleviate the volume changes during the charge/discharge processes, so that pulverization is prevented and the cycling life is prolonged. Third, the presence of the graphene, on the one hand, greatly enhances the conductivity of the composite, and on the other hand, it prevents the aggregation of the FL-GP.

4. Conclusion

In conclusion, we have successfully synthesized FL-GP/rGO, in which the ultrathin FL-GP was wrapped by electronically conductive rGO. Benefiting from the unique features of the FL-GP/rGO, the as-prepared samples demonstrated a high reversible capacity (504.2 mAh g^{-1} at the current density of 100 mA g^{-1} after 70 cycles without obvious capacity fading), remarkable rate performance (a reversible capacity of 230 mAh g^{-1} retained at 2 A g^{-1}), and superior cycling stability (a reversible capacity of 230 mAh g^{-1} still remaining after 250 cycles at 1 A g^{-1}) in the half cells. In addition, due to the high specific capacity, stable cycling performance, and appropriately low redox potential of the FL-GP/rGO, $Na_3V_2(PO_4)_3$//FL-GP/rGO full cells were assembled and demonstrated satisfactory electrochemical performance, indicating the potential for practical application of the as-reported anode materials.

Acknowledgements

F. Y. and J. H. contributed equally to this work. Financial support was provided by the Australian Research Council (ARC) (FT150100109, DP170102406, and CE140100012). The authors would like to thank the Electron Microscopy Centre (EMC) at the University of Wollongong for the electron microscopy characterizations and Dr. Tania Silver for critical reading of the manuscript and valuable remarks. F.Y. acknowledges the China Scholarship Council for his scholarship support. G.L. acknowledges the Australian Institute of Nuclear Science and Engineering (AINSE) Limited for financial assistance in the form of a Post Graduate Research Award (PGRA).

References:

[1] K. S. Novoselov, V. I. Fal'Ko, L. Colombo, P. R. Gellert, M. G. Schwab, K. Kim, *Nature* **2012**, *490*, 192.

[2] M. Chhowalla, H. S. Shin, G. Eda, L.-J. Li, K. P. Loh, H. Zhang, *Nat. Chem.* **2013**, *5*, 263.

[3] X. Zheng, P. Li, H. Zhu, K. Rui, G. Zhao, J. Shu, X. Xu, W. Sun, S. X. Dou, *Energy Storage Mater.* **2018**, *15*, 257.

[4] J. Liu, Y. Yang, P. Lyu, P. Nachtigall, Y. Xu, *Adv. Mater.* **2018**, *30*, 1800838.

[5] M. Osada, T. Sasaki, *J. Mater. Chem.* **2009**, *19*, 2503.

[6] A. K. Geim, *Science* **2009**, *324*, 1530.

[7] Y. Zhang, Y. W. Tan, H. L. Stormer, P. Kim, *Nature* **2005**, *438*, 201.

[8] L. R. Radovic, B. Bockrath, *J. Am. Chem. Soc.* **2005**, *127*, 5917.

[9] D. Hanlon, C. Backes, E. Doherty, C. S. Cucinotta, N. C. Berner, C. Boland, K. Lee, A. Harvey, P. Lynch, Z. Gholamvand, S. Zhang, K. Wang, G. Moynihan, A. Pokle, Q. M. Ramasse, N. McEvoy, W. J. Blau, J. Wang, G. Abellan, F. Hauke, A. Hirsch, S. Sanvito, D. D. O'Regan, G. S. Duesberg, V. Nicolosi, J. N. Coleman,

Nat. Commun. **2015**, *6*, 8563.

[10] L. Li, J. Kim, C. Jin, G. J. Ye, D. Y. Qiu, F. H. Da Jornada, Z. Shi, L. Chen, Z. Zhang, F. Yang, K. Watanabe, T. Taniguchi, W. Ren, S. G. Louie, X. H. Chen, Y. Zhang, F. Wang, *Nat. Nanotechnol.* **2017**, *12*, 21.

[11] L. Li, Y. Yu, G. J. Ye, Q. Ge, X. Ou, H. Wu, D. Feng, X. H. Chen, Y. Zhang, *Nat. Nanotechnol.* **2014**, *9*, 372.

[12] L. Li, W. Wang, P. Gong, X. Zhu, B. Deng, X. Shi, G. Gao, H. Li, T. Zhai, *Adv. Mater.* **2018**, *30*, 1706771.

[13] C. Barreteau, B. Michon, C. Besnard, E. Giannini, *J. Cryst. Growth* **2016**, *443*, 75.

[14] F. Shojaei, H. S. Kang, *Phys. Chem. Chem. Phys.* **2016**, *18*, 32458.

[15] W. Li, X. Li, J. Yu, J. Liao, B. Zhao, L. Huang, Ali Abdelhafiz, H. Zhang, J. H. Wang, Z. Guo, M. Liu, *Nano Energy* **2019**, *61*, 594.

[16] Y. Liu, Z. Sun, X. Sun, Y. Lin, K. Tan, J. Sun, L. Liang, L. Hou, C. Yuan, *Angew. Chemie Int. Ed.* **2020**, *59*, 2473.

[17] Y. Liu, Z. Sun, K. Tan, Di. K. Denis, J. Sun, L. Liang, L. Hou, C. Yuan, *J. Mater. Chem. A* **2019**, *7*, 4353.

[18] Y. Liu, Y. Fang, Z. Zhao, C. Yuan, X. W. (David) Lou, *Adv. Energy Mater.* **2019**, *9*, 1803052.

[19] Y. Wu, Y. Yu, *Energy Storage Mater.* **2019**, *16*, 323.

[20] J. Mao, T. Zhou, Y. Zheng, H. Gao, H. Liu, Z. Guo, *J. Mater. Chem. A* **2018**, *6*, 3284.

[21] K. Lee, S. Synnestvedt, M. Bellard, K. Kovnir, *J. Solid State Chem.* **2015**, *224*, 62.

[22] Y. Zhan, Z. Liu, S. Najmaei, P. M. Ajayan, J. Lou, *Small* **2012**, *8*, 966.

[23] Y. Liu, Z. Tai, J. Zhang, W. K. Pang, Q. Zhang, H. Feng, K. Konstantinov, Z. Guo, H. K. Liu, *Nat. Commun.* **2018**, *9*, 3645.

[24] K. S. Novoselov, *Science (80-.).* **2004**, *306*, 666.

[25] A. Ambrosi, Z. Sofer, M. Pumera, *Small* **2015**, *11*, 605.

[26] E. D. Grayfer, M. N. Kozlova, V. E. Fedorov, *Adv. Colloid Interface Sci.* **2017**, *245*, 40.

[27] B. Zhao, F. Chen, Z. Wang, S. Huang, Y. Jiang, Z. Chen, *Nanoscale* **2017**, *9*, 17922.

[28] H. Gao, T. Zhou, Y. Zheng, Q. Zhang, Y. Liu, J. Chen, H. Liu, Z. Guo, *Adv. Funct. Mater.* **2017**, *27*, 1702634.

[29] K. H. Nam, K. J. Jeon, C. M. Park, *Energy Storage Mater.* **2019**, *17*, 78.

[30] W. Li, L. Ke, Y. Wei, S. Guo, L. Gan, H. Li, T. Zhai, H. Zhou, *J. Mater. Chem. A* **2017**, *5*, 4413.

[31] F. Yang, H. Gao, J. Hao, S. Zhang, P. Li, Y. Liu, J. Chen, Z. Guo, *Adv. Funct. Mater.* **2019**, *29*, 1808291.

[32] Z. Li, L. Zhang, X. Ge, C. Li, S. Dong, C. Wang, L. Yin, *Nano Energy* **2017**, *32*, 494.

[33] X. Ge, Z. Li, L. Yin, *Nano Energy* **2017**, *32*, 117.

[34] M. Fan, Y. Chen, Y. Xie, T. Yang, X. Shen, N. Xu, H. Yu, C. Yan, *Adv. Funct.*

Mater. **2016**, *26*, 5019.

[35] Y. Von Lim, S. Huang, Y. Zhang, D. Kong, Y. Wang, L. Guo, J. Zhang, Y. Shi, T. P. Chen, L. K. Ang, H. Y. Yang, *Energy Storage Mater.* **2018**, *15*, 98.

[36] Z. Huang, H. Hou, C. Wang, S. Li, Y. Zhang, X. Ji, *Chem. Mater.* **2017**, *29*, 7313.

[37] C. Dong, L. Guo, Y. He, C. Chen, Y. Qian, Y. Chen, *Energy Storage Mater.* **2018**, *15*, 234.

[38] J. Qian, Y. Xiong, Y. Cao, X. Ai, H. Yang, *Nano Lett.* **2014**, *14*, 1865.

[39] A. Rudola, K. Saravanan, C. W. Mason, P. Balaya, *J. Mater. Chem. A* **2013**, *1*, 2653.

[40] J. Yang, H. Gao, S. Men, Z. Shi, Z. Lin, X. Kang, S. Chen, *Adv. Sci.* **2018**, *5*, 1800763.

[41] B. Cao, Q. Zhang, H. Liu, B. Xu, S. Zhang, T. Zhou, J. Mao, W. K. Pang, Z. Guo, A. Li, J. Zhou, X. Chen, H. Song, *Adv. Energy Mater.* **2018**, *8*, 1801149.

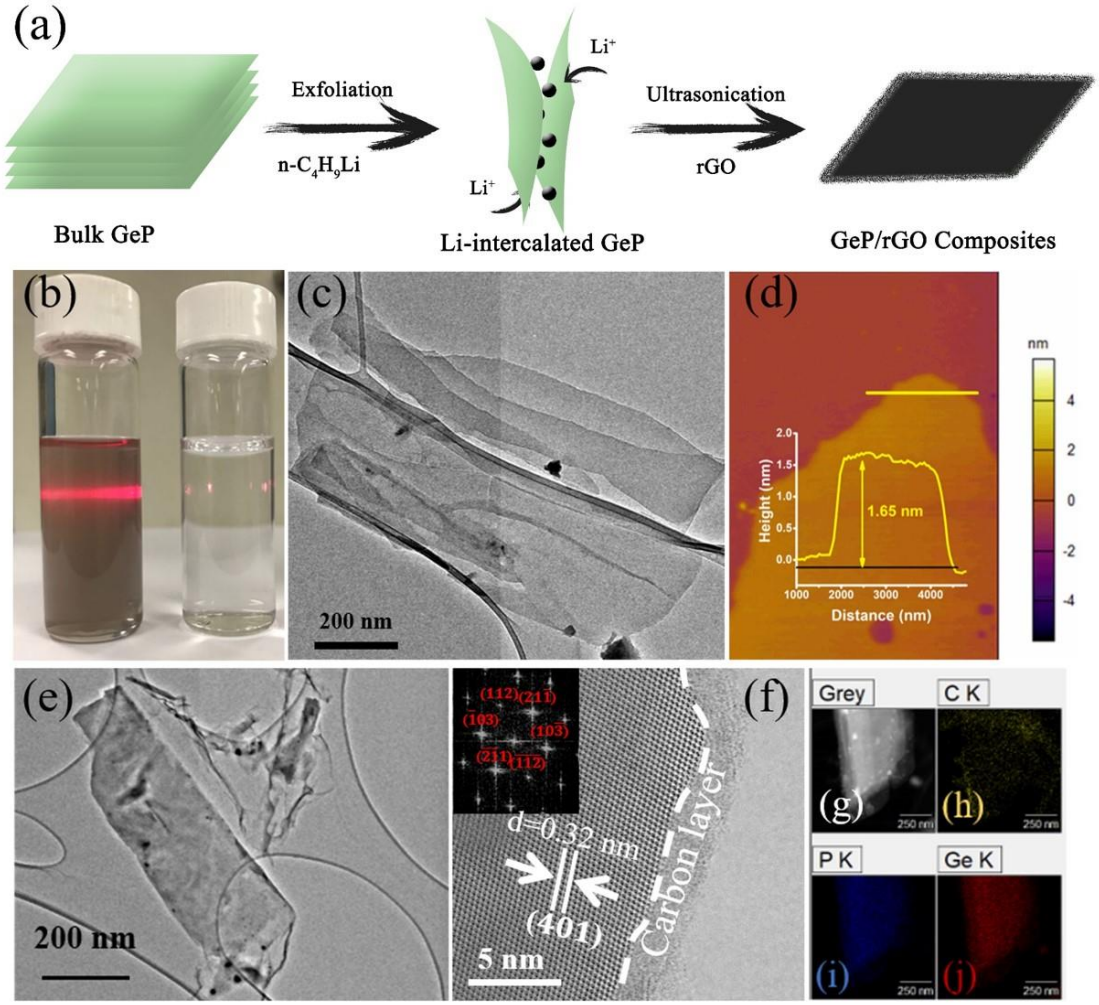

Figure 1. (a) The synthesis procedure for FL-GP/rGO; (b) Digital photograph of FL-GP (left) and blank DI water (right); (c) TEM image of FL-GP; (d) AFM image and corresponding height profile (inset) of the yellow line; (e) TEM image and (f) HRTEM image with the corresponding FFT pattern (inset) of the FL-GP/rGO nanosheets; (g, h, i, and j) elemental mapping analysis of FL-GP/rGO.

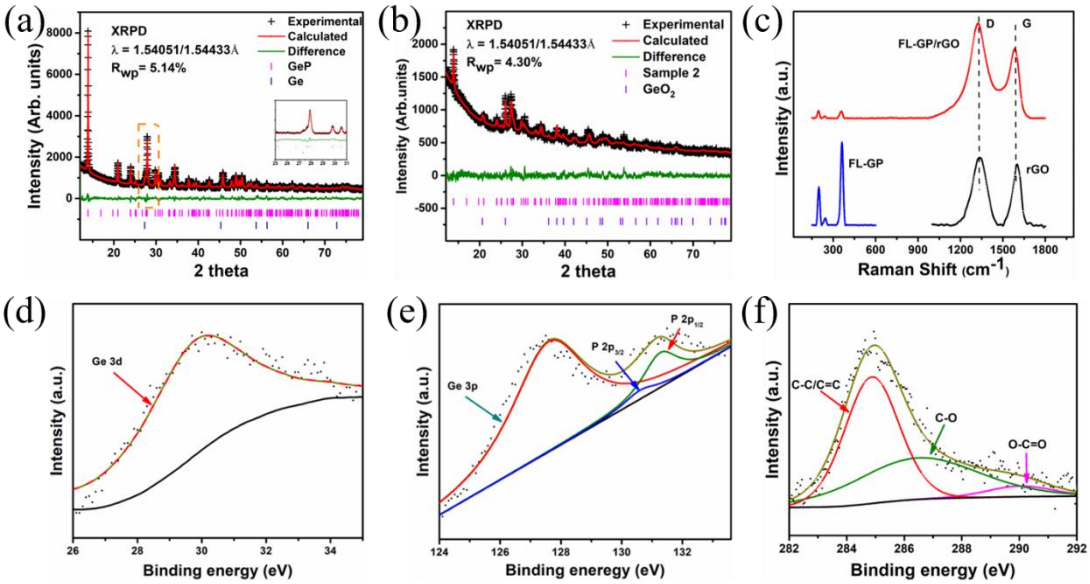

Figure 2. (a and b) Rietveld refinement patterns of the XRD results for bulk GeP (a) and FL-GP/rGO (b); (c) Raman spectra of FL-GP, rGO, and FL-GP/rGO nanosheets; (d, e, and f) XPS spectra of Ge (d), P (e), and C 1s (f) for FL-GP/rGO.

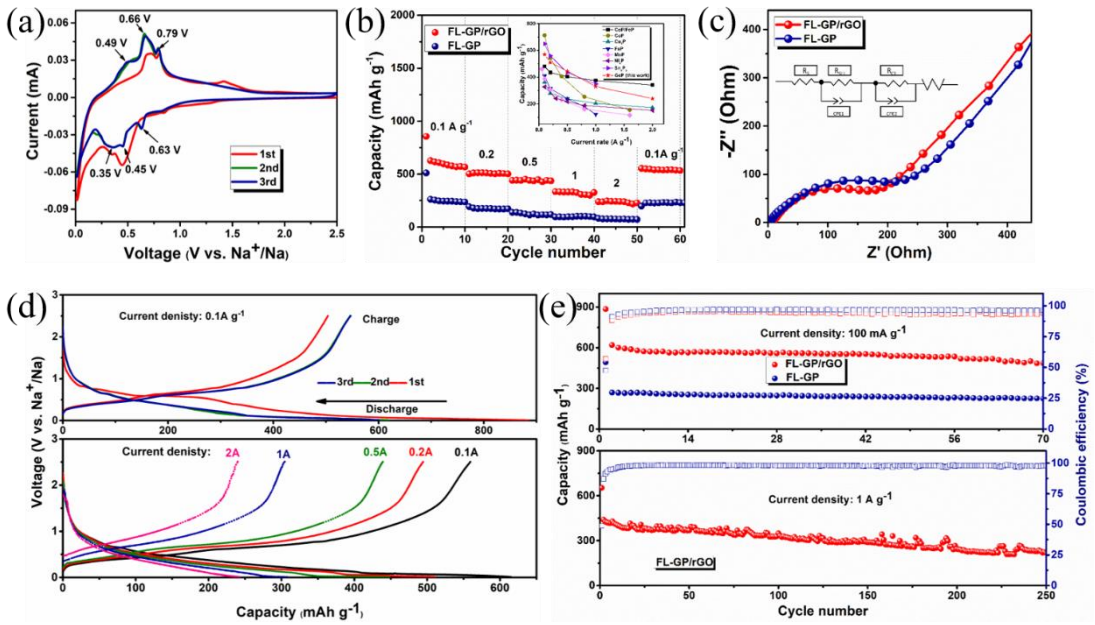

Figure 3. Half-cell electrochemical profiles of the as-prepared samples. (a) Cyclic voltammograms (CV) for the first three cycles of FL-GP/rGO; (b) Rate performances of FL-GP/rGO and FL-GP (inset: comparison of the rate capabilities of previously reported anode materials with our work); (c) Nyquist plots of the FL-GP/rGO and FL-GP, with the inset showing the equivalent circuit; (d) Charge-discharge voltage profiles for selected cycles of FL-GP/rGO under different current densities; (e) Cycling performances of FL-GP/rGO (0.1 and 1 A g^{-1}) and FL-GP (0.1 A g^{-1}).

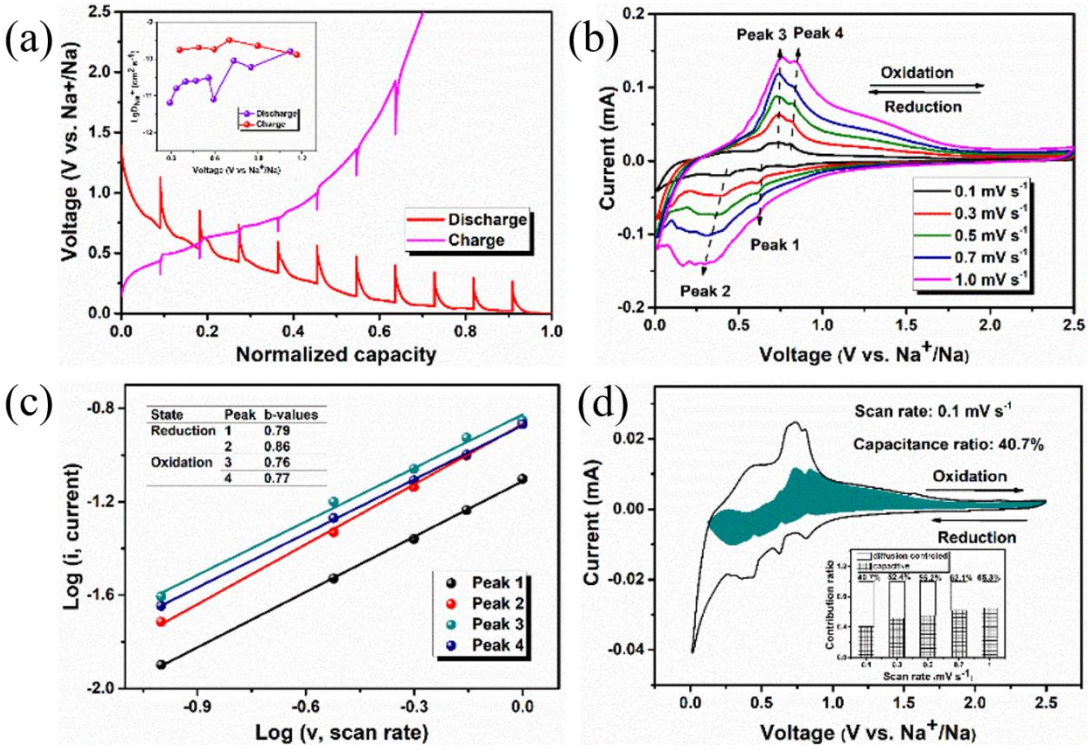

Figure 4. (a) Galvanostatic intermittent titration technique (GITT) curves of FL-GP/rGO for the charge and discharge processes. The inset shows the chemical diffusion coefficient of Na^+ ions as a function of voltage, as calculated from the GITT curves; (b) CV curves of FL-GP/rGO electrode at different scan rates; (c) log (*i*) versus log (*v*) plots at different redox states, where *i* is the peak current; (d) The calculated capacitance contribution (shadowed) area for the CV curve of the FL-GP/rGO nanosheet electrode, with the capacitance contributions at different scan rates shown in the inset.

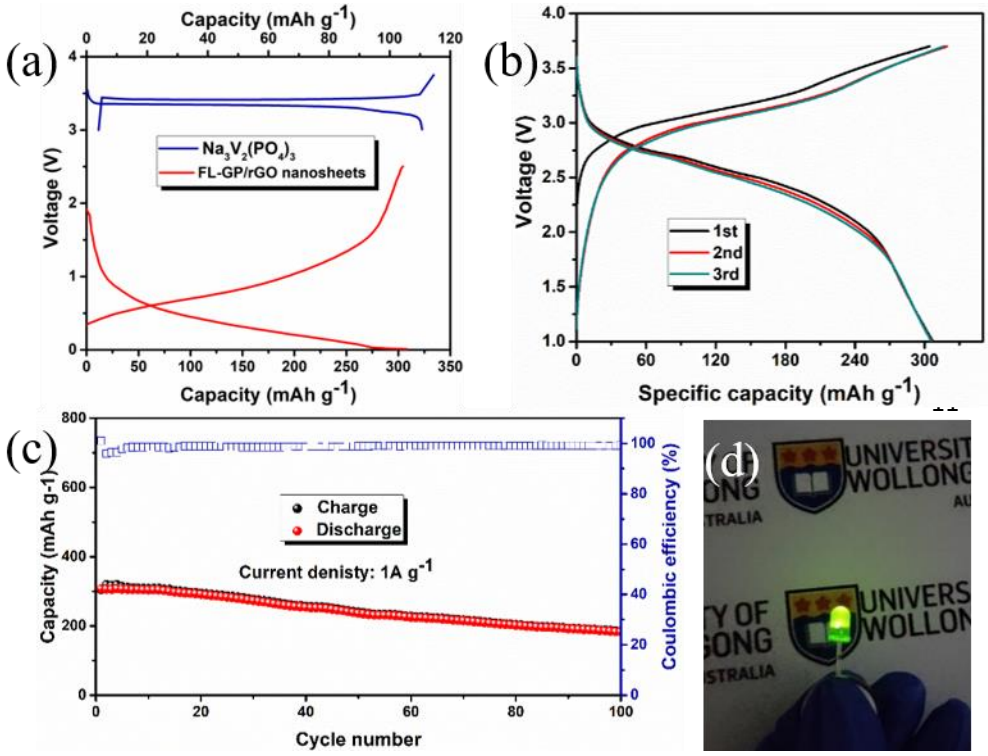

Figure 5. Electrochemical profiles of the sodium ion full cell batteries with $Na_3V_2(PO_4)_3$ as cathode and FL-GP/rGO as anode. (a) Typical charge/discharge curves of FL-GP/rGO anode and $Na_3V_2(PO_4)_3$ (NVP) cathode; (b) Charge/discharge curves of the FL-GP/rGO//$Na_3V_2(PO_4)_3$ full cells; (c) Cycling stability of the $Na_3V_2(PO_4)_3$//FL-GP/rGO full cells at 1 A g^{-1}; (d) Digital photograph showing that a full cell can light up an LED bulb.